Tungsten long-rod penetration into confined cylinders of boron carbide at and above ordnance velocities

L. Westerling*, P. Lundberg, B. Lundberg

Swedish Defense Research Agency, FOI, Weapons and Protection Division, S-14725 Tumba, Sweden

Abstract

The purpose was to investigate the influence of impact velocity and confinement on the resistance of boron carbide targets to the penetration of tungsten long-rod projectiles. Experimental tests with impact velocities from 1400 to 2600 m/s were performed using a two-stage light-gas gun and a reverse impact technique. The targets consisted of boron carbide cylinders confined by steel tubes of various thicknesses. Simulations were carried out using the AUTODYN-2D code and Johnson–Holmquist's constitutive model with and without damage evolution. The experimental results show that the penetration process had different character in three different regions. At low-impact velocities, no significant penetration occurred. At high-impact velocities, the relation between penetration velocity and impact velocity was approximately linear, and the penetration was steady and symmetrical. In between, there was a narrow transition region of impact velocities with intermittent and strongly variable penetration velocity. In the lower part of this region, extended lateral flow of the projectile took place on the surface of the target. The influence of confinement on penetration velocity was found to be small, especially at high-impact velocities. The simulated results for penetration velocity versus impact velocity agreed fairly well with the experimental results provided damage evolution was suspended below the transition region. © 2001 Elsevier Science Ltd. All rights reserved.

1. Introduction

The penetration capability of a modern long-rod projectile is so large that the weight required to defeat such a projectile using ordinary homogeneous steel armour would be unacceptable in

---

*Corresponding author. Tel.: + 46-8-55503000; fax: + 46-8-55504143.

E-mail address: larsw@sto.foa.se (L. Westerling).

Nomenclature

A static yield stress (Johnson–Cook)
B strain hardening coefficient (Johnson–Cook)
C strain rate coefficient (Johnson–Cook)
d external diameter of confinement tube
D damage variable (Johnson–Holmquist)
m thermal softening exponent (Johnson–Cook)
n strain hardening exponent (Johnson–Cook)
p pressure
P depth of penetration
R_t penetration resistance of target (Tate)
t time
T temperature
T_0 reference temperature (Johnson–Cook)
T_m melting temperature (Johnson–Cook)
u penetration velocity
v impact velocity
Y_p yield stress of projectile (Tate)
$\dot{\varepsilon}$ strain rate
$\dot{\varepsilon}_{p0}$ plastic strain rate threshold
$\dot{\varepsilon}_p$ plastic strain rate (Johnson–Cook)
ρ_0 reference density
ρ_p density of projectile material
ρ_t density of target material
σ yield stress (Johnson–Cook and Johnson–Holmquist)
σ_f yield stress of fully damaged material (Johnson–Holmquist)
σ_i yield stress of intact material (Johnson–Holmquist)

vehicle applications. This will be the case even more in the future when new acceleration techniques will considerably allow higher projectile velocities.

Ceramics have the potential to be used in highly weight-efficient armour systems not only for today's projectile velocities (1500–1800 m/s) but also for considerably higher impact velocities which are likely to be used tomorrow (2500–3000 m/s). See, e.g., [1].

The use of ceramics as armour materials has been studied extensively during the last decades. Some recent studies are [1–12]. Important mechanisms related to penetration of ceramics, such as development of cracks and fragmentation, are discussed in [2].

The purpose of this study was to obtain well-defined and time-resolved results for long-rod penetration in ceramics in order to enhance the understanding of processes which occur at different impact velocities, such as those of lateral flow of the projectile (interface defeat) and of intermittent and asymmetrical penetration.

Boron carbide was chosen as armour material as it is highly performing [8] and has a low density which facilitates high-quality X-ray registration of the projectile–target interaction. The influence of impact velocity of tungsten long-rod projectiles and target confinement on penetration velocity was investigated through both experimental tests and numerical simulations. First, the methods used in these studies will be presented. Then, the experimental and numerical results obtained will be compared with each other and with results obtained using Tate's model [13].

2. Experimental tests

The experimental tests were performed using a two-stage light-gas gun and a reverse-impact technique [9–12]. Thus, in each test a confined boron carbide cylinder target was launched against a stationary tungsten long-rod projectile suspended in thin cotton threads in front of the barrel. See Figs. 1 and 2.

The stationary projectiles were cylinders with length 150 mm and diameter 2 mm made of sintered tungsten alloy (DX 2 HCMF from Cime Bocuze). The boron carbide cylinders, with
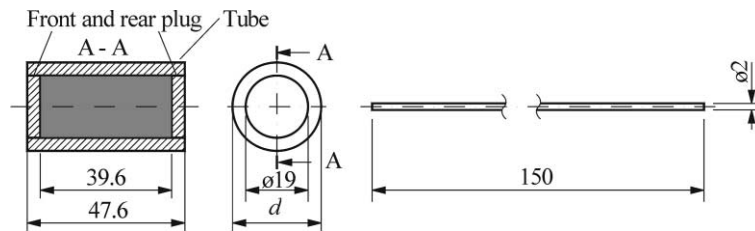

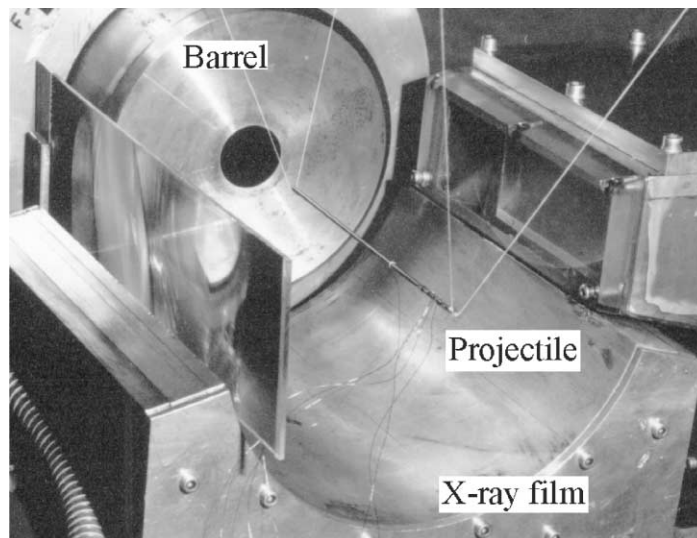Fig. 1. Targets and projectile for reverse impact tests. Dimensions in mm (d = 21, 23 and 27 mm).

Fig. 2. Experimental set-up.

nominal length 39.6 mm and diameter 19 mm (density 2490 kg/m^3, Vickers hardness 33 GPa) were cut from a single large sample and then ground to final shape. The confinement consisted of a tube with front and rear plugs locked by threads. Three different external diameters d of the tubes were used, viz., 21, 23 and 27 mm corresponding to 1, 2 and 4 mm wall thickness, respectively. The tube material was a tempered steel (SIS 2541-3, comparable to AISI/SAE 4340, flow stress 750 MPa). The internal diameter of the tube was slightly smaller (0.07 mm) than the diameter of the boron carbide cylinder. Therefore, the tube was heated to about 475°C before the boron carbide cylinder was inserted. The front and rear plugs were mounted after cooling and tightened with a torque of 24 Nm. Each target configuration was tested at nominal impact velocities of 1500 and 2500 m/s except that with 4 mm confinement, which was tested only at 1500 m/s.

Five 450 kV X-ray flashes, positioned at the same distance from the centre line but separated by 30°, were used to record the penetration process. In addition, two 150 kV X-ray flashes were used to determine the target velocity after the target–projectile interaction. This velocity was slightly lower than the initial target velocity but will be referred to as the impact velocity v. The X-ray flashes were triggered by means of a pulse caused by short circuit of two insulated copper wires (diameter 0.07 mm) glued on the front end of the projectile.

The penetration depth P in the boron carbide was determined from the X-ray pictures using image-processing techniques. The inaccuracy was estimated to be ± 0.20 mm. The instants of time t of X-ray pulses were measured within 0.1 μs. The average penetration velocities u over the observed time intervals were determined from the penetration versus time data using linear regression.

3. Simulations

The penetration processes were simulated with AUTODYN-2D, run as a Lagrangian code [14,15]. The boron carbide cylinder and the steel confinement including the front and rear plugs were modelled by joined subgrids, which means that the two materials were joined without the possibility to slide or separate. The tungsten projectile was modelled as a separate subgrid, and the interaction with the target was handled by the impact logic in AUTODYN (gap size 0.02 mm). Large deformations were treated by the method of erosion with the erosion strain set to 2.0 for boron carbide and to 1.5 for tungsten and steel. The grid consisted of rectangular zones of the same size in all subgrids, viz., 0.167 mm in the axial direction and 0.125 mm in the radial direction (6 and 8 zones per mm, respectively).

For boron carbide, Johnson–Holmquist's constitutive model [16] was used with yield stress

$$\sigma = (1 - D)\sigma_i(p, \dot{\varepsilon}) + D\sigma_f(p, \dot{\varepsilon}), \tag{1}$$

where $D \in [0,1]$ is the damage parameter, σ_i the yield stress of the intact material ($D = 0$) and σ_f is the yield stress of the fully damaged material ($D = 1$). These yield stresses are functions of the hydrostatic pressure p and the strain rate $\dot{\varepsilon}$. The constitutive parameters are defined in the appendix, and their values, also due to Johnson–Holmquist [16], are given in Table 1. For tungsten and steel use was made of Mie–Grüneisen and linear equations of state, respectively, and

Table 1
Parameters for boron carbide used in Johnson–Holmquist's model

Parameter	Notation	Values in [16]	Values used in AUTODYN
Density (kg/m³)	ρ_0	2510	2510
Bulk modulus (GPa)	$K = K_1$	233	233
Coeff. for 2nd degree term in EOS (GPa)	K_2	−593	−593
Coeff. for 3rd degree term in EOS (GPa)	K_3	2800	2800
Shear modulus (GPa)	G	197	197
Hugoniot elastic limit (HEL) (GPa)	HEL	19.0	19.0
Effective stress at HEL (GPa)	σ_{HEL}	15.44	—
Pressure at HEL (GPa)	p_{HEL}	8.71	—
Volumetric strain at HEL	μ_{HEL}	0.0408	—
Intact strength coefficient	A	0.927	0.9637
Intact strength exponent	N	0.67	0.67
Strain rate coefficient	C	0.005	0.005
Fracture strength coefficient	B	0.70	0.7311
Fracture strength exponent	M	0.85	0.85
Maximum fracture strength	S_{fmax}	0.2	0.2045
Damage coefficient	D_1	0.001	0.001
Damage exponent	D_2	0.5	0.5
Bulking factor	β	1.0	1.0
Tensile strength (GPa)	σ_{hyd}	0.26	0.26

Johnson–Cook's constitutive model [17] with yield stress

$$\sigma = (A + B\varepsilon_p^n)\left(1 + C\ln\left(\frac{\dot{\varepsilon}_p}{\dot{\varepsilon}_{p0}}\right)\right)\left(1 - \left(\frac{T - T_0}{T_m - T_0}\right)^m\right), \tag{2}$$

where ε_p is plastic strain, $\dot{\varepsilon}_p$ is plastic strain rate, T is temperature, and A, B, C, m, n, $\dot{\varepsilon}_{p0}$, T_0 and T_m are parameters. Values of the parameters were obtained from the material library in AUTODYN and are given in Table 2. These values can also be found in [17,18]. The density of tungsten, however, was obtained from the supplier.

All cases tested were simulated. For 2 mm confinement, additional simulations were carried out for the impact velocities 800, 1000, 1200, 2000, 2200 and 2400 m/s. For 2 mm confinement simulations were also carried through with the damage evolution suspended in Johnson–Holmquist's model. In these simulations, the impact velocities were 800, 1000, 1200 and 1400 m/s.

4. Results and discussion

X-ray pictures of the penetration process at the impact velocities 1454 m/s (Test 5) and 1502 m/s (Test 1) are shown in Figs. 3(a) and (b), respectively. An interesting effect at the lower of these impact velocities is extended lateral flow on the surface of the boron carbide in the early stage of the

Table 2
Parameters for tungsten and steel

Parameter	Notation	Tungsten	Steel
Density (kg/m^3)	ρ_0	17600	7830
Bulk modulus (GPa)	K	—	159
Bulk sound speed (m/s)	c_0	4029	—
Slope in U_s versus U_p diagram	s	1.237	—
Grüneisen coefficient	Γ	1.54	—
Shear modulus (GPa)	G	160	81.8
Static yield limit (GPa)	A	1.506	0.792
Strain hardening modulus (GPa)	B	0.177	0.51
Strain hardening exponent	n	0.12	0.26
Strain rate coefficient	C	0.016	0.014
Plastic strain rate threshold (1/s)	$\dot{\varepsilon}_{p0}$	1.0	1.0
Thermal softening exponent	m	1.0	1.03
Reference temperature (K)	T_0	300	300
Specific heat (J/kg K)	C_v	134	477
Melting temperature (K)	T_m	1723	1793

penetration process. This effect, which is also called interface defeat, was first reported by Hauver and co-workers [19]. At this impact velocity and confinement thickness (2 mm), the penetration process starts with extended lateral flow, continues with the formation of a wide crater, and is completed with the production of a narrow crater. At the slightly higher of these impact velocities, the penetration channel is narrow in some parts and wide in others which indicates intermittent penetration.

X-ray pictures of the penetration process at the significantly higher impact velocities 1581 m/s (Test 6) and 2500 m/s (Test 8) are shown in Figs. 4(a) and (b), respectively. At these impact velocities, the penetration processes are relatively steady and symmetrical. Also, they are strikingly similar to each other despite the substantial difference in impact velocity.

Experimental results for penetration versus time, evaluated from the X-ray pictures, and corresponding results from simulations are shown in Fig. 5. At higher impact velocities (1787–2601 m/s), there is a fair agreement between the measured and simulated penetrations. At lower impact velocities (1427–1480 m/s), however, the penetrations obtained from simulation with damage evolution are much larger than those evaluated from experimental tests.

Experimental results for penetration velocities, evaluated by linear regression for each case of test and simulation, and impact velocities are given in Table 3. As in Tests 5 and 11, the penetrations evaluated from the tests deviated significantly from linear dependence on time, two penetration velocities were evaluated, one for early time and another for late.

Experimental results for penetration velocity versus impact velocity are shown in Fig. 6. It can be seen that the relation between penetration velocity and impact velocity has different character in different regions. At low-impact velocities, the penetration velocity is zero or near zero. At high-impact velocities, the relation between penetration velocity and impact velocity is approximately linear in accordance with previous results for boron carbide [12]. Between these two regions,

(a)

| 9.5 μs | 15.7 μs | 36.4 μs | 46.4 μs |

(b)
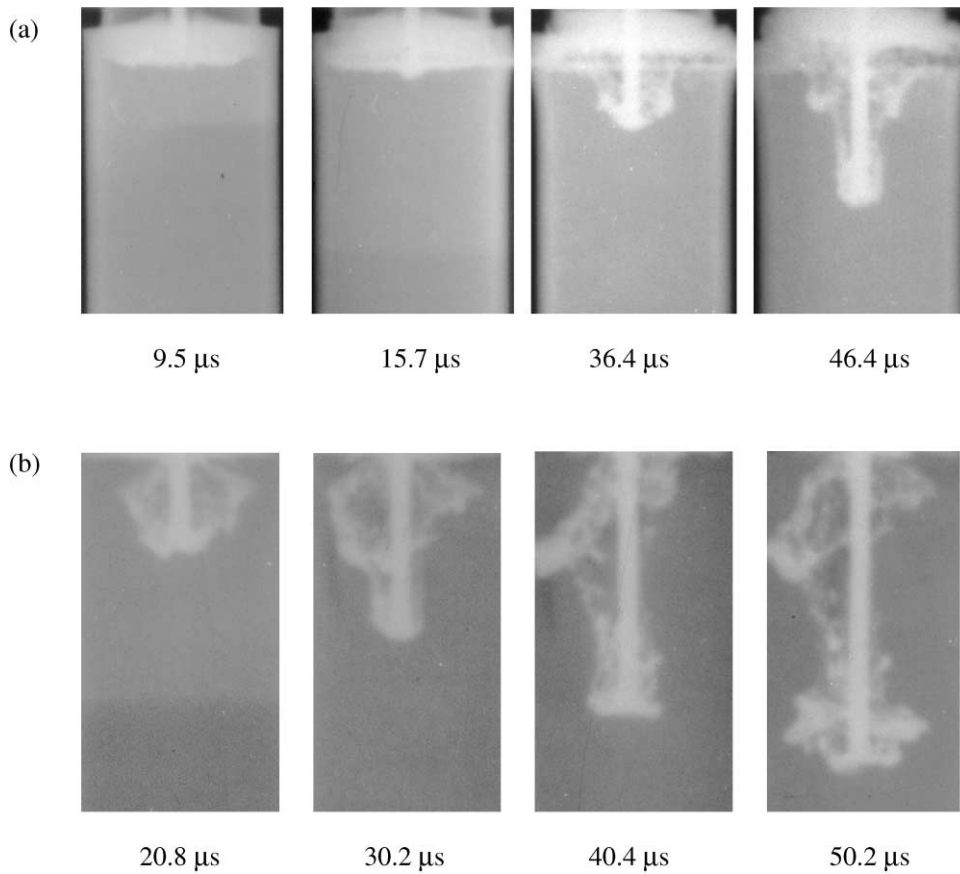

| 20.8 μs | 30.2 μs | 40.4 μs | 50.2 μs |

Fig. 3. X-ray pictures from (a) Test 5 (1454 m/s) and (b) Test 1 (1502 m/s) at four instants of time after impact.

there is a narrow transition region of impact velocities with a rapid increase of penetration velocity. This distinct behaviour in the transition region may be due to a large variation in target resistance which corresponds to the large variation in crater width shown by the X-ray pictures of Fig. 3.

The influence of confinement thickness on penetration velocity is small at high-impact velocities. In the transition region, the results of Fig. 6 indicate that the penetration velocity may be somewhat higher with 2 mm than with a 4 mm confinement. A similar indication is given by the results of simulations in Table 3. A possible interpretation is that a thicker confinement maintains the maximum penetration resistance which boron carbide can provide at a given impact velocity for a longer time.

By using Tate's relation [13]

$$\tfrac{1}{2}\rho_p(v-u)^2 + Y_p = \tfrac{1}{2}\rho_t u^2 + R_t, \tag{3}$$

between penetration velocity u and impact velocity v, we can estimate the variation of target penetration resistance R_t within the transition region. In this relation, ρ_p and Y_p are the density and yield stress of the projectile, and ρ_t is the density of the target. This relationship is shown in Fig. 6 for two different values of $R_t - Y_p$ which, according to the results of the tests, correspond to
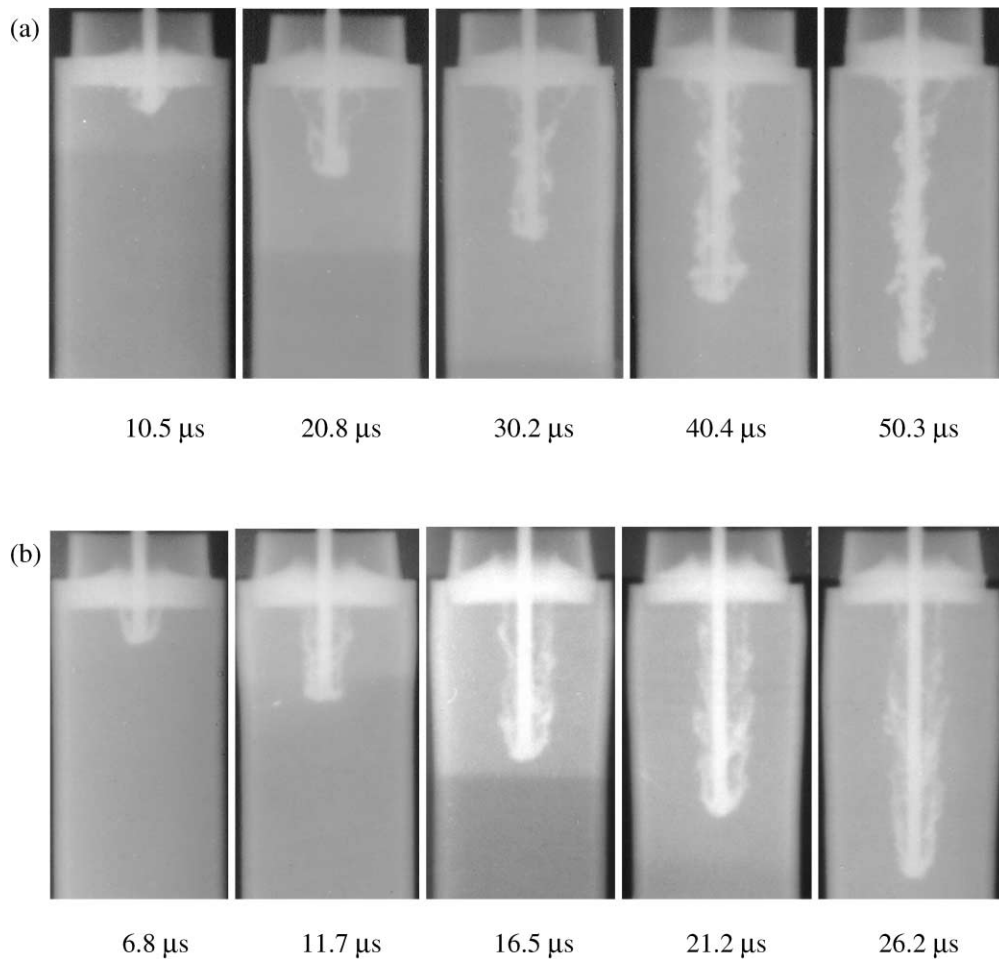
Fig. 4. X-ray pictures from (a) Test 6 (1581 m/s) and (b) Test 8 (2500 m/s) at five instants of time after impact.

the lower and upper ends of the transition region. With the assumption that the projectile strength is constant and equal to $Y_p = 2\,\text{GPa}$ at the high strain rates at hand, the target penetration resistance would vary between $R_t = 6.2$ and $18.5\,\text{GPa}$ through the transition region. Thus, the strong variation of penetration velocity might be attributed to a penetration resistance which is strongly variable within the transition region but nearly constant in the region of high-impact velocities. Similar results for the latter region, but with slightly lower $R_t - Y_p$, have been reported in [12]. One reason for the difference could be that the qualities of the boron carbide were not the same. A difference in quality is indicated by the material hardness, which was 21 GPa Knoop (1 kg) in [12] compared to 33 GPa Vickers (1 kg) in this study.

Fig. 7 shows penetration velocity versus impact velocity from tests and simulations with 2 mm confinement as well as the two extreme curves based on Tate's model. The penetration velocity evaluated from simulations using Johnson–Holmquist's model with damage evolution (black triangles) agrees reasonably well with the experimental results (open triangles) for impact velocities
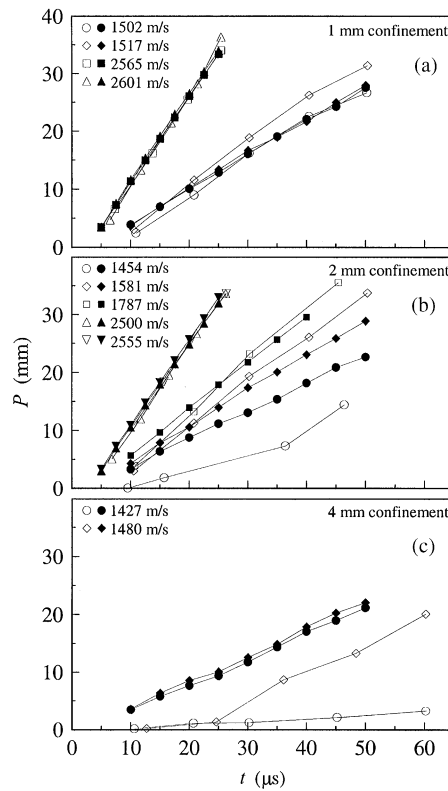
Fig. 5. Penetration P versus time t for different impact velocities according to experimental tests (open symbols) and simulations (solid symbols) with (a) 1, (b) 2 and (c) 4 mm confinement.

Table 3
Impact and penetration velocities in experimental tests and simulations

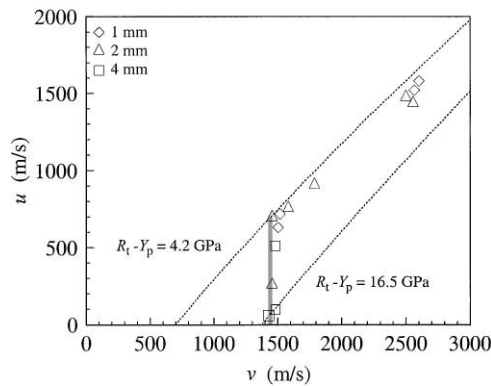| Test no.	Confinement (mm)	Symbols used in Figs. 6 and 7	Impact velocity v (m/s)	Penetration velocity u (m/s)	
				Test	Simulation
1	1	◇	1502	630	590
2	1	◇	1517	720	600
3	1	◇	2565	1520	1495
4	1	◇	2601	1580	1520
5	2	△	1454	270, (710, $t > 36\,\mu s$)	480
6	2	△	1581	770	615
7	2	△	1787	920	795
8	2	△	2500	1485	1440
9	2	△	2555	1450	1480
10	4	□	1427	60	445
11	4	□	1480	100, (510, $t > 27\,\mu s$)	465

Fig. 6. Penetration velocity u versus impact velocity v for different confinements according to experimental tests. Shaded area shows transition region. Curves according to Tate [13].
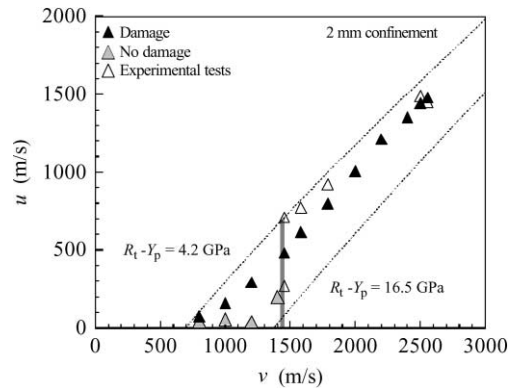
Fig. 7. Penetration velocity u versus impact velocity v for 2 mm confinement with (▲) and without (△) damage evolution and corresponding results according to experimental tests (△). Shaded area shows transition region. Curves according to Tate [13].

above the transition region. However, the results of simulation do not show the strong variation of penetration velocity in the transition region which can be observed in the experimental results. For this reason, a few simulations with damage evolution suspended were performed for impact velocities below the transition region. The results of these simulations (grey triangles) show low penetration velocities in accordance with the experimental tests.

5. Conclusions

The experimental results show that the penetration process had a different character in the three different regions. At low-impact velocities, no significant penetration occurred. At high-impact velocities, the relation between penetration velocity and impact velocity was approximately linear, and the penetration was steady and symmetrical. In between, there was a narrow transition region of impact velocities with intermittent and strongly variable penetration velocity. In the lower part of this region, extended lateral flow of the projectile took place on the surface of the target. The influence of confinement on penetration velocity was found to be small, especially at high-impact velocities. The simulated results for penetration velocity versus impact velocity agreed fairly well with the experimental results provided damage evolution was suspended below the transition region.

Appendix A. Parameters in Johnson–Holmquist's constitutive model

In order to define the parameters in Table 1 and make it possible to discuss some problems with input values for AUTODYN, the main formulas in Johnson–Holmquist's constitutive model for brittle materials [16] are given here. The yield stresses for intact and fully damaged materials are

given as functions of pressure p and strain rate $\dot{\varepsilon}$ by

$$\sigma_{\mathrm{i}}(p,\dot{\varepsilon}) = A\sigma_{\mathrm{HEL}}\left(\frac{\sigma_{\mathrm{hyd}}+p}{p_{\mathrm{HEL}}}\right)^{N}\left(1 + C\ln\left(\frac{\dot{\varepsilon}}{\dot{\varepsilon}_0}\right)\right), \tag{A.1}$$

$$\sigma_{\mathrm{f}}(p,\dot{\varepsilon}) = B\sigma_{\mathrm{HEL}}\left(\frac{p}{p_{\mathrm{HEL}}}\right)^{M}\left(1 + C\ln\left(\frac{\dot{\varepsilon}}{\dot{\varepsilon}_0}\right)\right) \leqslant S_{\mathrm{fmax}}\sigma_{\mathrm{HEL}} \tag{A.2}$$

respectively, where A, N, C, B, M, S_{fmax} are dimensionless parameters, σ_{hyd} is the tensile strength, and $\dot{\varepsilon}_0$ is the threshold strain rate for strain rate effects. The parameters σ_{HEL}, p_{HEL}, and HEL (not used in Eqs. (A.1–A.3)) are the von Mises effective stress, the pressure, and the axial stress, respectively, at the Hugoniot elastic limit. For partly damaged material, the yield stress is given by $\sigma = (1 - D)\sigma_{\mathrm{i}} + D\sigma_{\mathrm{f}}$, where $D \in [0,1]$ is a damage parameter which is incremented in each time step by the ratio between the plastic strain increment and a pressure dependent failure strain

$$\varepsilon_{\mathrm{f}}(p) = D_1\left(\frac{\sigma_{\mathrm{hyd}}+p}{p_{\mathrm{HEL}}}\right)^{D_2}, \tag{A.3}$$

where D_1 and D_2 are dimensionless parameters. The equation of state gives the pressure as the sum of a third-degree polynomial in the compressive volumetric strain and a term which takes care of a fraction β of the released elastic energy due to damage increase. In tension only the linear term is retained in the polynomial.

In [16] the normalisation constants σ_{HEL} and p_{HEL} (as well as μ_{HEL}) were calculated from HEL by using the non-linear equation of state and the shear modulus. In AUTODYN, they are calculated from the input value HEL $= 19.0\,\mathrm{GPa}$ by using the linear approximations

$$\sigma_{\mathrm{HEL}} = \frac{2G}{K + (4/3)G}\,\mathrm{HEL}, \quad p_{\mathrm{HEL}} = \frac{K}{K + (4/3)G}\,\mathrm{HEL}. \tag{A.4}$$

This leads to the values $\sigma_{\mathrm{HEL}} = 15.10\,\mathrm{GPa}$ and $p_{\mathrm{HEL}} = 8.93\,\mathrm{GPa}$, which differ from those in Table 1 (even their ratio differs). In the expression for the yield strength of the intact material, (A.1), p_{HEL} and σ_{HEL} appear only in the coefficient $A\sigma_{\mathrm{HEL}}/p_{\mathrm{HEL}}^N$, which will get a value consistent with the data of Table 1 if the parameter A is given the new value $A = 0.9638$. Similarly, $B\sigma_{\mathrm{HEL}}/p_{\mathrm{HEL}}^M$ and $S_{\mathrm{fmax}}\sigma_{\mathrm{HEL}}$ in Eq. (A.2) will be invariant if B and S_{fmax} are given the new values $B = 0.7311$, $S_{\mathrm{fmax}} = 0.2045$. The original value was used for the coefficient D_1 in Eq. (A.3) as the correction would have been only about one percent and its value is not very accurately known.

For the simulations with damage evolution suspended, we made a user subroutine defining the yield stress for the undamaged material given by Eq. (A.1). We first, unsuccessfully, tried to suspend the damage evolution by setting the coefficient D_1 in the expression for the fracture strain in Eq. (A.3) to a large number. However, occasional negative pressures caused the fracture strain in (A.3) to be zero which lead to damage.

References

[1] Hohler V, Stilp AJ, Weber K. Hypervelocity penetration of tungsten sinter-alloy rods into alumina. Int J Impact Engng 1995;17(1–6):409–18.

[2] Shockey DA, Marchand AH, Skaggs SR, Cort GE, Burkett MW, Parker R. Failure phenomenology of confined ceramic targets and impacting rods. Int J Impact Engng 1990;9(3):263–75.

[3] Franzen RR, Orphal DL, Anderson Jr. CE. The influence of experimental design on depth-of-penetration (DOP) test results and derived ballistic efficiencies. Int J Impact Engng 1997;19(8):727–37.

[4] Woodward RL, Gooch Jr. WA, O'Donnell RG, Perciballi WJ, Baxter BJ, Pattie SD. A study of fragmentation in ballistic impact of ceramics. Int J Impact Engng 1994;15(5):605–18.

[5] Anderson Jr. CE, Royal-Timmons SA. Ballistic performance of 99.5%-Al_2O_3 ceramic tiles. Int J Impact Engng 1997;19(8):703–13.

[6] Lundberg P, Westerling L, Lundberg B. Influence of scale on the penetration of tungsten rods into steel-backed alumina. Int J Impact Engng 1996;18(4):403–16.

[7] Westerling L, Lundberg P, Holmberg L, Lundberg B. High velocity penetration of homogenous, segmented and telescopic projectiles into alumina targets. Int J Impact Engng 1997;20:817–27.

[8] Ernst HJ, Hoog K. Protective power of several ceramics, correlated to some static material parameters. Proceedings of the 13th International Symposium on Ballistics, vol. 3. Stockholm (Sweden): 1993: p. 119–26.

[9] Subramanian R, Bless SJ. Penetration of semi-infinite AD995 alumina targets by tungsten long rod penetrators from 1.5 to 3.5 km/s. Int J Impact Engng 1995;17:807–16.

[10] Orphal DL, Franzen RR, Piequtowski AJ, Forrestal MJ. Penetration of confined aluminum nitride targets by tungsten long rods at 1.5 to 4.5 km/s. Int J Impact Engng 1996;18(4):355–68.

[11] Orphal DL, Franzen RR. Penetration of confined silicon carbide targets by tungsten long rods at impact velocities from 1.5 to 4.6 km/s. Int J Impact Engng 1997;19(1):1–13.

[12] Orphal DL, Franzen RR, Charters AC, Menna TL, Piequtowski AJ. Penetration of confined boron carbide targets by tungsten long rods at impact velocities from 1.5 to 5.0 km/s. Int J Impact Engng 1997;19(1):15–29.

[13] Tate A. Further results in the theory of long rod penetration. J Mech Phys Solids 1969;17:141–50.

[14] Birnbaum NK, Cowler MS, Itoh M, Katayama M, Obata H. AUTODYN — an interactive non-linear dynamic analysis program for microcomputers through supercomputers. Ninth International Conference on Structural Mechanics in Reactor Technology. Lausanne (Switzerland): August 1987.

[15] Birnbaum NK, Cowler MS. Numerical simulation of impact phenomena in an interactive computing environment. International Conference on Impact Loading and Dynamic Behaviour of Materials "IMPACT 87". Bremen (Federal Republic of Germany): May 1987.

[16] Johnson GR, Holmquist TJ. Response of boron carbide subjected to large strains, high strain rates, and high pressure. J Appl Phys 1999;85(12):8060–73.

[17] Johnson GR, Cook WH. A constitutive model and data for metals subjected to large strains, high strain rates, and high temperatures. Proceedings of the Seventh International Symposium on Ballistics. Holland: 1983. p. 541–47.

[18] van Thiel M, Shaner J, Salinas E, Michels T, MacNaughton C. Compendium of Shock Wave Data, Vol. 1. Sec. A-1. Lawrence Radiation Laboratory, University of California, Livermore, UCRL-50108, 1977. p. 230–31.

[19] Hauver GE, Netherwood PH, Benck RF, Kecskes LJ. Ballistic performance of ceramic targets. Army Symp Solid Mech USA: 1993.